Climate pattern scaling set for an ensemble of 22 GCMs – adding uncertainty to the IMOGEN vn 2.0 impacts system

Przemyslaw Zelazowski[1,2], Chris Huntingford[3], Lina M Mercado[4,3] and Nathalie Schaller[1,5]

[1]Oxford University Centre for the Environment, University of Oxford, Oxford, OX1 3QY, UK

[2]Centre of New Technologies, University of Warsaw, Warsaw, 02-097, Poland

[3]Centre for Ecology and Hydrology, Wallingford, OX10 8BB, UK

[4]Geography, College of Life and Environmental Sciences, University of Exeter, Exeter, EX4 4RJ, UK

[5]Center for International Climate and Environmental Research (CICERO), Oslo, NO-0318, Norway

Correspondence to: Chris Huntingford (chg@ceh.ac.uk)

Abstract. Global Circulation Models (GCMs) are the best tool to understand climate change, as they attempt to represent all the important Earth system processes, and including anthropogenic perturbation through fossil fuel burning. However, GCMs are computationally very expensive, which limits the number of simulations that can be made. Pattern-scaling is an emulation technique that takes advantage of the fact that local and seasonal changes in surface climate are often approximately linear in amount of warming over land and globe. This allows interpolation away from a limited number of available GCM simulations, to assess alternative future emissions scenarios. In this paper we present a pattern-scaling set consisting of spatial climate change patterns along with parameters for an energy balance model that calculates the amount of global warming. The set is derived from 22 GCMs of the WCRP CMIP3 database, setting the basis for similar eventual pattern development for CMIP5 ensemble. Critically, it extends the use of the IMOGEN (Integrated Model Of Global Effects of climatic aNomalies) framework to enable scanning across full uncertainty in GCMs for impacts studies. Across models, the presented climate patterns represent consistent global mean trends, with maximum four GCMs exhibiting opposite sign of the trend per variable (relative humidity). The described new climate regimes are generally warmer, wetter (but with less snowfall), cloudier and windier, and with decreased relative humidity. Overall, when averaging individual performance across all variables, and without considering co-variance, the patterns explain one-third of regional change in decadal averages (mean Percentage Variance Explained, PVE, 34.25±5.21), but signal in some models exhibits much more linearity (e.g. MIROC3.2(hires):41.53) than in others (GISS_ER: 22.67). The two most often considered variables: near-surface temperature and precipitation have a PVE of 85.44±4.37 and 14.98±4.61, respectively. The dataset is available for download and researchers in the areas of ecosystem modelling and climate change impact assessment are already starting to use it. Besides allowing time-efficient assessment for non-standard future scenarios of changed greenhouse gas (GHG) concentrations, it enables understanding of new representations of land surface processes, and including climate-carbon cycle feedbacks. Current and potential future applications of such modelling system are discussed.

1 Introduction

Global Climate Models (GCMs) are the primary source of our understanding of and ability to estimate future climate regimes resulting from anthropogenic Greenhouse Gas emissions (GHGs). However, the use of these tools is limited by their requirements for computing power, and the complexity of the task, in particular in the case of multi-model assessments. "Pattern-scaling" (Huntingford & Cox 2000, Mitchell et al 2003), is a methodology that takes advantage of the fact that, to a reasonable approximation, local and seasonal changes in surface climate are linear in amount of warming over land and globe. It allows interpolation away from a limited number of available GCM simulations, enabling a time-efficient assessment of surface meteorological changes for alternative non-standard future scenarios of changed GHG concentrations. This can include, for example, new scenarios that fall between the current Representative Concentration Pathways (RCP, Taylor et al., 2012), and potentially to investigate pre-defined future temperature thresholds such as two degrees.

"Climate-change patterns" (or "patterns") are coefficients of the regression between mean warming over Earth's land regions, ΔT_l (K) and local changes in surface climatology. They are derived by comparison against outputs from GCMs, and presented as local monthly mean changes over land per degree of mean global over land. "Pattern-scaling" is a simple procedure in which these patterns are multiplied by ΔT_l to give local changes in climatology. A global Energy Balance Model (EBM; e.g. Wigley et al. 2000) is then applied to model how the GHG concentrations translate into changes in radiative forcing, Q (Wm^{-2}) and then into temperature increase over land regions (ΔT_l).

The IMOGEN framework (Integrated Model Of Global Effects of climatic aNomalies; Huntingford et al. 2010) is a computationally efficient tool for modelling impacts of future climate change on terrestrial ecosystems. It consists of the JULES land surface model (Best et al., 2011; Clark et al., 2011) linked to a pattern-scaling module (Huntingford and Cox, 2000). The scaling provides monthly mean changes in climate variables over land, notably temperature, relative humidity, precipitation and radiation - quantities used to drive ecosystem models. In addition, a simple oceanic global carbon cycle model is included (Joos et al., 1996 and Appendix of Huntingford et al., 2004), which expands the typical usage of patterns-scaling by allowing consideration of oceanic climate-carbon cycle feedbacks, alongside land-based feedbacks. All simulations use an hourly time step and a spatial resolution of 2.5° latitudinal x 3.75° longitudinal, or 72 by 96 grid boxes, as in the UKMO-HadCM3 GCM. Over land, but excluding Antarctica, this corresponds to 1631 grid-boxes. Linking forcings to mean warming over land, ΔT_l, is achieved with the EBM which requires five parameters, described in the Methods section. The relevant equations are presented in Huntingford and Cox (2000). The five parameters are referred to as IMOGEN EBM calibration parameters (or simply "calibration parameters"), and, as in the case of patterns, they are also derived from GCM runs. The "patterns" and "calibration parameters" together form a "patterns-scaling set".

IMOGEN was originally established to allow rapid assessment of a range of alternative GHG emission scenarios, e.g. corresponding to the standard Special Report on Emissions Scenarios, (SRES, Nakićenović et al, 2000) or Representative Concentration Pathways (RCP, Taylor et al., 2012) where GCM simulations are unavailable, as well as interpolating away from what GCM simulations do exist to new user-prescribed emissions or concentration pathways. RCPs were used to

inform the recent 5th IPCC report (IPCC, 2013), via the set of climate model simulations available at that time in the CMIP5 dataset (Taylor et al 2012). CMIP5 has evolved further since year 2013 and to hold more simulations; the exercise to calibrate a patterns-scaling set for CMIP5 is under way. Normally, evolving atmospheric carbon dioxide (CO_2) concentrations are calculated as a consequence of prescribed CO_2 emissions, along with prescription of non-CO_2 forcings for other GHGs and aerosols. Then an overall radiative forcing Q is calculated to drive the EBM. Alternatively, all radiative forcing Q can be prescribed directly as future forcings' pathways, in which case CO_2 concentrations are prescribed, again for scenarios that differ from the standard ones.

In practise, though, IMOGEN has been used more to assess the effects of new parameterisations, adjustment or inclusion of new processes into the land surface model. This is as a precursor for any eventual inclusion of land surface model improvements in a full GCM. IMOGEN allows easy and fast assessment of ranges of parameterisations, numerical stability checks and critically the relative importance of new understanding of ecological and hydrological responses globally, and including feedbacks on the carbon cycle. Examples include the impacts of changes in diffuse radiation on the land carbon sink (Mercado et al., 2009), or the effects of ozone damage on plant productivity (Sitch et al 2007).

Until recently, these offline studies were performed with patterns of climate change from a single model, UKMO-HadCM3 (IMOGEN version 1.0, Huntingford et al., 2010). The purpose of this paper is to present a patterns-scaling set which emulates a broad range of GCMs, and nearly the complete set of those held in the WCRP CMIP3 database (Meehl et al., 2007). This extends the use of IMOGEN for assessment of climate change, or land surface response, to scan across uncertainty in climate models. Such uncertainty can then be evaluated against any further uncertainty in any terrestrial surface impacts of interest. In Section 2 we describe the methods which lead to the patterns-scaling set. Section 3 describes the actual set, including discussion of found inter-GCM differences, and we include metrics describing the accuracy of the linearity assumption of meteorological changes against level of global warming, as implicit in the scaling method. Section 4 reviews existing applications of the IMOGEN pattern-scaling system and comments on the future benefits of inclusion of our climate model uncertainty. Finally, Section 5 discusses the strengths and caveats of the pattern-scaling approach.

2. Data and Methods

2.1 The WCRP CMIP3 multi-model dataset and data pre-processing

Spatial patterns (i.e. maps) of climate change and energy balance model calibration parameters (together forming the "climate-patterns set") are derived from GCM data available through the World Climate Research Programme Coupled Model Intercomparison Project, phase three (WCRP CMIP3; Meehl et al., 2007). The WCRP CMIP3 multi-model dataset resulted from an international effort to run a coordinated set of twentieth- and twenty-first-century climate GCM simulations for a small prescribed number of future scenarios, covering many aspects of climate variability and change. All these simulations were subsequently analysed and formed the basis of much that is reported in the Fourth Assessment (AR4) of the

Intergovernmental Panel on Climate Change (IPCC, 2007). The dataset consists of data from 24 GCMs, representing 17 modelling groups from 12 countries. The climate patterns set presented here (Table 1) corresponds to 22 GCMs, because GISS_AOM is an atmosphere-ocean model without surface meteorological projections over land and key data from CGCM3.1(T63) GCM were missing (see below). In the case of GISS-EH and GISS-ER GCM, WCRP CMIP3 data were supplemented with the formally associated pool provided by National Aeronautics and Space Administration Goddard Institute for Space Studies (http://data.giss.nasa.gov/pub/pcmdi).

The analysed model runs represent scenarios of four types: (i) control experiments: either pre-industrial or present day (Picntrl, or Pdcntrl), (ii) the idealized 1% yr^{-1} CO_2 increase up to doubled and quadrupled levels (1pctto2x, 1pctto4x), (iii) the twentieth-century run (20C3M) representing modelled period from pre-industrial to present-day and (iv) the high- (A2) and mid-emission (A1B) future scenarios defined by the Special Report on Emission Scenarios (SRES, Nakicenovic et al. 2000). When multiple simulations are available of any particular scenario, then the analysis is limited to the first available, as the inter-run variability has been reported to be small (Frieler et al 2012).

Variables analysed for each GCM are those representing land surface climatology: 1.5 m air temperature (TAS), 1.5 m relative humidity (HURS), 10 m wind speed (UAS and VAS, combined into direction-less UA), precipitation (PR, including snow PRSN), downward shortwave (RSDS) and long-wave (RLDS) radiation fluxes and surface pressure (PS). The codes in brackets are the name conventions used in the WCRP database for individual variables. It is these variables that are required to run the JULES land surface scheme inside the IMOGEN framework. Additionally, Net Radiative Flux at the top of the atmosphere (positive downwards); Top of Model (RTMT); is also processed, as this is required to drive the global energy balance model.

There were some discrepancies between data requirements to run the IMOGEN system and the actual data availability in WCRP CMIP3. They are listed in Table 1. For all GCMs, surface relative humidity (HURS) data was not available, but a 4D representation of this variable at pre-defined pressure levels (HUR) was generally available. This allowed extrapolation of surface relative humidity from two highest available pressure levels which are near the land surface. In the case of INGV-SXG, PCM and CCSM3 GCMs, surface wind was obtained in the same procedure. For two cases, the required surface data was available, but suffered from quality and other issues. In UKMO-HadGEM1 data, last month of the SRES A2 simulation was missing (and in this study it was filled-in with interpolated values), and surface wind data was presented on non-standard grid (and it was interpolated onto a standard UKMO-HadGEM1 grid). For MRI-CGCM2.3.2, many values in snow precipitation data (PRSN) were missing (the data were not used in this study) and there was no land mask available (SFTLF, later obtained from the Japanese modelling group). Finally, in the case of four GCMs certain non-critical variables were entirely missing (Table 1).

GCMs differ significantly between each other in the spatial grid resolution and generally how they represent the Earth surface's detail (as represented in the "land mask" variable SFTLF which reports gridbox land fraction). Spatial resolution varies between hundreds of kilometres (e.g. GISS models, or INM-CM3.0) to *c*. 100 km (e.g. MIROC3.2hires model, mid-

latitudes, Table 1). Data are mapped on either a regular or a Gaussian grid, and gridbox classification into land and water is either binary (either 100% or 0%) or continuous, with only a part of GCMs explicitly depicting freshwater bodies in their land masks. This diversity of output spatial properties alone imposes a challenge for data end-users, including policymakers, especially when it comes to multi-model assessments of a pre-defined geographical domain. To force our common land

5   surface model within the IMOGEN system using alternative GCM-based estimates of climate change, we harmonised all types of WCRP CMIP3 grids into one, which was chosen to be the UKMO-HadCM3. This ensures compatibility with previous applications of the IMOGEN tool, with resolution of 2.5° latitudinal x 3.75° longitudinal. The common grid allows, in a systematic way, to capture the impact of climate uncertainty that remains within GCMs. More information about this re-gridding procedure is provided in the Supplementary Material.

10   **2.2 Climate pattern scaling set and post-processing**

The presented climate patterns are a set of regression coefficients, each representing the change per degree of mean global warming over land, while the fitting is done with decadal average changes against the global mean warming over land, as predicted by each GCM. The simple form of the analogue model for an anomaly (Δ) in one of the considered land surface variables V in the climate regime in the decade c can be described as:

15   $$\Delta V(c,g,m,i) = \Delta T_l(c,i)V_x(g,m,i) \tag{1}$$

where the anomaly is linked to a single location on the UKMO-HadCM3 grid (g), month of the annual cycle (m), GCM (i) and decadal time index (c). Regressions to find patterns V_x use global land warmings ΔT_l directly from original GCMs, but when the IMOGEN model is used predictively, then these values are derived using an Energy Balance Model (EBM) component (see below).

20   Regressing local climate with mean land warming is done with the assumption that climate is stable before the anthropogenic impact. This implies that the regression line starts at the origin of the coordinate system, so the intercept equals zero, and there is a fit with just one regression co-efficient, the slope. This starting point is represented by an average of three decades from the twentieth-century run (20C3M, years 1961-1990, Figure 1, panel C) which is a period corresponding to the Climate Research Unit's Time Series 2.1 (CRU TS 2.1) dataset describing Earth's climatology (or "climate normals", Mitchell and

25   Jones 2005). In the WCRP CMIP3 dataset, the historical 20C3M GCM simulations are normally followed by a future transient run, driven by one of SRES scenarios that describe potential pathways ahead in emissions. In the presented work, for most of GCMs, a high-emissions "business-as-usual" SRES A2 run was analysed, while in a few cases when these data were not available the SRES A1B run was used (Table 2), which represents relatively lower levels of warming (Nakicenovic et al. 2000).

30   Emulating an ensemble of GCMs requires that the relationship between anthropogenic climate forcings, global warming and warming over land is established for each GCM separately. . The EBM, described in full in Huntingford and Cox (2000), requires the fitting of five calibration parameters to a simple global energy balance model: (i) an ocean effective thermal

diffusivity, κ (Wm^{-1}K^{-1}), (ii) a constant ratio of mean land and ocean surface (SST) rate of warming, v, (iii-iv) climate sensitivity over land λ_l and ocean λ_o (W m^{-2} K^{-1}), and (v) land fraction f (variable SFTLF, including Antarctica). All the energy retained in the planetary system, and as seen in any difference in top-of-the-atmosphere radiation, is assumed to enter the oceans in a diffusive process, and thus changing SSTs and then ΔT_1 via v. Estimation of EBM parameters was done by

5   fitting them against an independent set of scenarios: the idealised CO_2 increase scenario (1pctto2x or 1pctto4x), preceded by a control experiment: (Picntrl or Pdcntrl). Subsequently, functioning of the parameterised EBM was validated – that is, it was used predictively - against data from one of the available runs corresponding to SRES scenarios (SRES A2 or SRES A1B, Table 2). Figure 1 illustrates the key components of the process of deriving a pattern-scaling set in the case of the UKMO-HadGEM1 GCM.

10   In general, our climate patterns represent absolute changes. However, for precipitation, we make one additional calculation which results in data normalisation. This is to circumvent the problem of particularly large biases in the description of the current precipitation regime by some GCMs (Ines and Hansen 2006). For each calculated precipitation pattern (ΔP), this is then multiplied by the ratio of the observed precipitation ($P_{\text{CRU\_XXc}}$) from the CRU TS 2.1 dataset (Mitchell and Jones 2005) and the one simulated by the GCM ($P_{\text{GCM\_XXc}}$) for the control period. This follows Ines and Hansen (2006), and Malhi et al.

15   (2009):

$$\Delta P'(g,m,i) = \Delta P(g,m,i) \times \frac{P_{\text{CRU}_{\text{XXc}}}(i,m_S,g_S)}{P_{\text{GCM}_{\text{XXc}}}(i,m_S,g_S)} \tag{2}$$

Furthermore, the adjustment of Eqn. (2) was performed for each grid box g, month m and GCM i, after smoothing in time and space (averaging over the grid box and its immediate neighbourhood: g_S, and across three months m_S). This reduce significantly the number of artefacts caused by occasional division by near 0. The remaining few cases of high and low

20   divergence (i.e. $P_{\text{CRU,XXc}}/P_{\text{GCM,XXc}}$) were capped at 5 and 0.2. Snow was scaled according to the same scaling factor as total precipitation. The final patterns set is available in two versions: with precipitation normalised by Eqn. (2), and without this.
As a last step, in four cases when available GCMs data had one or two non-key variables missing (Table 1), the gaps were filled in with across-ensemble means.

3 Results

25   **3.1 Energy balance parameters**

The five key EBM parameters are presented in Table 2. In most cases (17) climate sensitivity over ocean (λ_o, Wm^{-2}K^{-1}) is higher than over the land (λ_l, Wm^{-2}K^{-1}). The reverse trend is well pronounced in three models (CSIRO-Mk3.5, MIROC3.2highres, MRI-CGCM2.3.2). Climate sensitivity over land varies five-fold between models and is the lowest in ECHO-G, UKMO-HadCM3, CGCM3.1(T47) and the highest in BCCR-BCM2.0, PCM, FGOALS-g1.0, although 2/3rds of

30   the models have a much narrower range 0.9-1.7 Wm^{-2}K^{-1}. The most varying variable is ocean diffusivity (κ, Wm^{-1}K^{-1}),

which determines the ability of the ocean to extract heat from the climate system through diffusion. Even after excluding the two most extreme cases, the range remains high: from 270 (HadCM3, CGCM3.1(T47)) to 2800 $Wm^{-1}K^{-1}$ (CSIRO-Mk3.0). The most extreme value of 11000 $Wm^{-1}K^{-1}$ is for the FGOALS-g1.0 GCM, which clearly stands out from the ensemble. This spread reflects the fact that a full understanding of oceanic flows and deeper overturning, which affects mean vertical heat transport, is still required to reduce model spread. In comparison, the land/ocean temperature increase contrast (ν) is a remarkably stable parameter, with a range 1.40-1.78 across all models.

3.2. Patterns across models, space and seasons

Across models, patterns of particular variables represent consistent trends when averaged spatially and across months (Table 3), with maximum four exceptions per variable (relative humidity), i.e. cases when average pattern is of opposite sign than in the majority of GCMs. The patterns capture the nature of a new emerging climate regimes, which can be characterised as warmer, wetter (but with less snowfall), cloudier and windier, with decreased relative humidity, and increased atmospheric pressure. Globally, relative humidity stands out as the variable with the highest uncertainty in the magnitude of change, with SD across the models exceeding the mean. In the case of other variables apart from longwave downward radiation and air temperature near surface (RLDS, TAS, with very small spread) the magnitude of standard deviation is similar (62-88 % of the mean).

In the case of each GCM, the patterns represent a unique regional and seasonal distribution of change in surface climatology in a greenhouse-gas enriched atmosphere. To present these differences, we focus on two of the strongest drivers of terrestrial ecosystems change (and co-incidentally, which are also having the largest influence on society in general) – that is adjustments to temperature and precipitation. The annual mean rate of warming per degree of global warming over land (Figure 2) in some models is much more evenly distributed geographically (e.g. BCCR-BCM2.0) than in others (e.g. NCAR-PCM1). However, all of the models exhibit the majority of warming in Northern latitudes. The smallest warming occurs in tropical Africa and Asia, while in tropical South America the magnitude is much more uncertain. The spatial pattern of warming is either well stratified with latitude (e.g. FGOALS-g1.0 model), or more nuanced (GISS models). The patterns of precipitation change (Figure 3) are more complex and in some regions they exceed the uncertainty in regional warming (e.g. South America); however, in other areas the signal is very consistent, such as drying of Southern Europe.

Across-model seasonal averages (Figure 4 and 5, for temperature and precipitation respectively) reveal a more spatially and temporally consistent picture than when considering models individually. These figures show that the majority of warming occurs on Northern latitudes during colder seasons. Moreover, there is a strong summer warming trend over mid-West North America, Mediterranean region, Middle East and Central Asia. The seasonal patterns of precipitation change appear as linked to those of temperature, but are generally more uncertain. Winter warming in the North is accompanied by more precipitation which contrasts with lower summer warming and reduced rainfall. Changes in tropical rainfall appear as much

more uncertain. Western and Central Africa north of equator is a zone with particularly high uncertainty regarding summer warming.

Stippling in Figure 5 provides additional measure of uncertainty - it indicates when there is agreement in 90% of the models, as to whether precipitation is going to increase or decrease. This is the case over most of the land area and seasons. However, in many dry areas and seasons where this measure is not robust due to low precipitation levels (and the signal is difficult to detect), the agreement is uncertain. Some areas stand out in this regard: large parts of South America in northern winter and summer, high northern latitudes in the summer and central Asia in autumn. That rainfall changes remain a large uncertainty in climate model projections is noted in the 4th IPCC report (IPCC 2007).

3.3. Performance of linear approximation assumption in "pattern-scaling" for individual variables

The robustness of climate patterns is assessed by their ability to reproduce the decadal GCM data. It varies widely between variables, which can be split into four categories, according to the mean Percentage Variance Explained (PVE) metric (Table 3), a simple way to assess each variable separately through the analysis of decadal means against the pattern. The most robust are the patterns which represent the drivers of global warming: temperature TAS and long-wave radiation RLDS (PVE 85.44±4.37, and 84.74±4.97, respectively). The next group consists of variables, which explain around one quarter of variance: short-wave radiation RSDS and air pressure PS. Variables linked to availability of water: precipitation PR, snowfall PRSN, relative humidity HURS, form the third group (PVE 14.98±4.61, 17.96±4.67, 16.92±5.71, respectively). The last category is represented by wind patterns (of combined variables UAS and VAS), which represent only 7.11±3.32 PVE. Wind patterns also contain the highest proportion of negative PVE (4.9%).

Overall (i.e. when per-variable results are averaged, without considering co-variance), climate patterns explain one-third of regional climate change (PVE 34.25±5.21); however, signal in some models exhibits much more linearity (e.g. MIROC3.2(hires): 41.53) than in others (GISS_ER: 22.67). These estimates exclude cases where the PVE statistic could not be calculated due to either a lack of data (2.8%, Table 1), or null (e.g. short-wave radiation during polar night) and extremely low values (e.g. precipitation in the dry season), accounting for 6.7% of cases.

In terms of spatial distribution of robustness of the two key variables: temperature and precipitation (Figure 6), it is generally the opposite. For temperature, lower PVE values occur in the North, with minimum over Greenland and North-West North America (but still above 50%). The highest values occur across the Tropics. In the case of precipitation, the highest PVE occurs over the northern latitudes (above 50°N), particularly in Asia. In some Tropical areas (sub-saharan Africa, South-East Amazon) areas with relatively robust signal (PVE ~20%) are adjacent to regions where the robustness could not be estimated due to very small and erratic rainfall in the dry season.

4. Applications

The "pattern-scaling" concept was originally designed as a tool for scientists to inform policymakers, enabling investigation of expected changes in surface climatology for a broader range of scenarios of atmospheric greenhouse gas concentrations than available in archived GCM runs. The original version of a framework capturing, in effect an interpolation methodology, was based around UKMO-HadCM3 GCM (Huntingford and Cox, 2000). Once the IMOGEN system (Huntingford et al., 2010) linked such scaling of meteorological drivers to force directly a land surface model, the main application of such framework has been to undertake global analyses of ecosystem response in a changing climate. Particular examples include quantification of wetland methane feedbacks (Gedney et al., 2004), the impacts of changes in diffuse radiation to the land carbon sink (Mercado et al., 2009), the effects of tropospheric ozone on plant productivity (Sitch et al., 2007), the significance of energy crop planting on future atmospheric CO_2 concentration (Hughes et al., 2010) and how alternative mixtures of changes in atmospheric composition, even corresponding to identical radiative forcing changes, can have very contrasting impacts on land surface carbon stocks (Huntingford et al., 2011).

The potential for Amazon forest collapse, or "die-back", remains an iconic concern for potential climate change impacts. Such a possibility has been identified in a combined climate-carbon cycle climate model UKMO-HadCM3LC (Cox et al 2000, 2004). Later, the robustness of predictions of Amazon 'dieback' were investigated with IMOGEN (version 1.0) and the original UKMO-HadCM3 patterns (Huntingford et al. 2008), by analysing the vegetation response to (i) some limited uncertainty via prescribed bounds in the parameterisations of the atmospheric component of UKMO-HadCM3 (related to HadCM3LC), (ii) description of canopy radiation interception – "big leaf" versus "multilayer" and (iii) representation of vegetation dynamics using an area based model and an individual based model. All simulations show a fairly robust dieback. More recently, a set of the climate patterns described in this paper were used to analyse the potential for tropical rainforest "die back". Zelazowski et al. (2011) combined the patterns and global contemporary climatology to produce high resolution maps of the future extent of humid tropical forests, while Huntingford et al. (2013b) forced the IMOGEN framework with the full set of patterns. Both studies found that models other than UKMO-HadCM3 are less likely to project such losses, which reflects the particularly stronger climatic signal for the Amazon region temperature and precipitation changes for UKMO-HadCM3, as noted in Figures 2 and 3 above.

In order to exemplify the ability of IMOGEN to project changes to impacts, we report results of the mean annual total runoff (R_{tot}, mm day^{-1}) simulation (Figure 7), and compare them directly to GCM estimates of change. In Figure 7, for SRESA1B emissions scenario, we consider the ability of IMOGEN to project runoff changes and compare the result to such changes taken directly from the GCMs themselves. Hence this is comparing the IMOGEN simulations that emulate multiple GCMs but with a single land surface model (JULES), versus runoff values directly from the GCMs. The latter therefore contain alternative estimates of climate change, and additionally the responses of different land surface models. During modelled pre-industrial period, and modelled period centred on year 2090, total runoff values are recorded for each GCM (both emulated in IMOGEN, and directly from GCMs). Then in each case, the change is calculated. In the top panels, the mean of

these changes are shown, whilst the bottom panels are the standard deviations of these change values. Although there are similarities between left and right-hand panels (over northern latitudes, in particular), there are important differences too (notably the drying signal in GCM output for Africa and Australia is not reflected by the IMOGEN framework). For SDs, in some locations there is higher variability for IMOGEN than for the GCMs themselves; however, this pertains mainly to the

5   regions where IMOGEN predicts higher runoff.. The latter may be surprising, as considering that GCMs directly introduce another level of uncertainty i.e. inter-land surface model differences. Our finding is suggestive that JULES has a particularly sensitive response of runoff to imposed climatic changes. Looking ahead to new forms for IMOGEN, one possibility to additionally capture the different land surface responses is to pattern-scale directly impact variables of interest such as runoff.

10 Runoff provides a challenge for comparison, as it is frequently a relatively small number between two larger fluxes of precipitation and evapotranspiration (transpiration, plus soil evaporation and interception loses) and so sensitive to change in those fluxes. Direct comparison also needs to account for IMOGEN being initialised with a climatology based on the CRU dataset, and temporal dis-aggregation to sub-daily drivers of JULES having not been calibrated against any particular GCM. Nevertheless, to be a useful tool for impacts assessment, then IMOGEN must capture the general features of GCM

15 projections when operated for similar emissions scenarios.

Whilst IMOGEN framework allows testing hypotheses in more advanced land surface configurations, such as JULES (Mercado et al., 2007), the major advantage of routine utilisation of the full set of patterns described in this paper is that any assessment of uncertainty in how the land surface may function, for different levels of atmospheric greenhouse gases, can be now understood in the context of the full spectrum of uncertainty implicit in climate models from different GCM research

20 centres. To aid this even further, ultimately the analysis of Sitch et al. (2008), in which the IMOGEN system is used to diagnose uncertainty in representation of future plant biogeography and climate-carbon cycle feedbacks using five Dynamical Global Vegetation Models (DGVMs), but combined with only a single set of climate models patterns based on UKMO-HadCM3, can be re-visited. If each DGVM modelling centre could operate their latest DGVM configuration, across the range of emulated GCMs, then this would give a fuller estimate of the balance between implications of uncertainty in

25 climate and uncertainty in terrestrial ecosystem response and its feedbacks on the global carbon cycle.

In some regards, land surface models in GCMs are still in their infancy, considering the growing knowledge of how vegetation responds physiologically to imposed climatic changes. For this reason, there are many future plans to use IMOGEN as an intermediate step, before inclusion in a full GCM, to test and demonstrate the relative importance of a particular new understanding. For example, we have used the patterns derived on this paper on an analysis of the sensitivity

30 of the future land carbon storage to thermal acclimation of plant photosynthesis (Mercado et al., in preparation). This is a noted major deficiency in current large-scale terrestrial models (Booth et al 2012; Huntingford et al., 2013a; Smith and Dukes 2013). In addition, the assessment of newly available enhanced description of leaf dark respiration (Atkin et al., 2015) is needed, as well as the inclusion of both Nitrogen and Phosphorus constraints to plant productivity in tropical ecosystems

(e.g. Mercado et al., 2011), and inclusion of a full representation of a coupled Carbon-Nitrogen cycle in JULES (Zaehle et al 2010). Furthermore, it is desirable to test the effects of adding height competition into the vegetation dynamics module of JULES, in order to add ecological succession modelling (Smith et al 2001; Moorecroft et al 2001), along with assessing the impacts of improved representation of stomatal conductance (Medlyn et al 2011; Kala et al 2015) and plant hydraulics (Sperry et al. 2015) on simulated land carbon- and water-cycles to climate. The later could extend as far as testing any hormonal signalling in the hydraulic linkages between soil moisture and stomata response; an effect well known by the physiological community but hereto never tested in a full large-scale gridded land surface model (Huntingford et al., 2015). Finally, impacts of introducing a better representation of plant functional types and plant trait variation across space and time (Verheijen et al 2015) on simulated land carbon should also be considered.

5. Discussion

In this paper we present a "pattern scaling set", consisting of spatially explicit climate change patterns and EBM calibration parameters, which together represent 22 GCMs of the WCRP CMIP3 database (Meehl et al., 2007). This data set extends the use of the IMOGEN climate impacts assessment tool to scan across uncertainty in climate models. Despite relying on a set of simple assumptions, the tool can capture a significant part of the predicted changes in surface climatology. Terrestrial ecosystem response studies can use this modelling framework to gain new insights into how the land surface component of the Earth system functions.

An important aspect of the presented work is the comprehensive study of pattern's robustness, i.e. their ability to capture variability of climate simulated by GCMs. The fact that together the set of considered variables capture 1/3rd of decadal variability in monthly averages, suggests that it is a technique with a significant potential, especially since it allows a large reduction in input data and computation requirements through removal of the time dimension. Overall, the presented patterns are in good agreement with the results presented in the Fourth Assessment Report of the Intergovernmental Panel on Climate Change (see SI and Figure 10.9 in Meehl et al., 2007). This applies to both the multi-model mean changes in surface climate, as well as the degree of agreement between the models (stippling in Figure S3).

However, the ability of climate patterns to capture the course of changes varies significantly between the modelled climate variables. In contrast to temperature change (85.44±4.37% of variability explained by climate patterns), change in precipitation, which is amongst critical aspects of climate change, is generally relatively difficult to capture in this linear methodology. Into a large extent this is a consequence of the fact that the original GCM results are also relatively inconsistent as regards precipitation. In climate patterns this uncertainty is further exacerbated, and in consequence overall 85% of variability remains unexplained, although it should be noted that in some regions seasonal precipitation patterns explain up to 75% of variability (generally at high northern latitudes). The very poor performance in precipitation estimation over dry zones is in part because it is not possible to capture the trend through what are very low precipitation levels. In these

areas, the mean change over decades gives low PVE values, as any change in very small current absolute precipitation can result in high relative deviations from preindustrial levels. In such circumstances, precipitation is very much dominated by inter-annual fluctuations which mean scaling cannot be captured well.

The presented work is an attempt to unify the spatially heterogeneous GCM data resource. Placing on a common grid brings
5   strong benefits to the IMOGEN tool. However as a result of the applied procedure for re-gridding combined with land mapping (see Supplementary Material), the calculated regional patterns represent areas that are comprised fully of land, while in much of original GCM data grid-boxes represents a mix of land and ocean. The total land fraction in the presented spatial patterns is slightly increased, mainly because some mixed land/ocean areas are replaced by land-only estimates to match the UKMO-HadCM3 grid with grid-boxes of either pure land or ocean (see Figure S1). This increases the average
10 grid-box warming, due to diminished representation of the oceanic heat uptake. As a result, the fitting procedure yields regional warming patterns (column "TAS" in Table 3) which, when area-weighted, overall return a value slightly larger than 1.0 K/K. However, this effect has no impact on the global energy budget in the IMOGEN framework, which is resolved independently with EBM.

There are a number of potential methodological enhancements that can be implemented in the next version of the dataset
15 including the way it is utilised by the IMOGEN framework. For example, so far the natural variability around the trend in IMOGEN is simulated through a daily "weather generator" component, under the assumption that the spread remains within the set bounds. However in reality the signal in GCM runs can not only adjust the mean but also the variability itself. This suggests that future research, at least for some variables, additional patterns might be needed that capture variability changes. Furthermore, an extra set of patterns to capture longer-term inter-annual or inter-decadal variability, over and beyond linear
20 changes, could be considered. Model outputs have, until recently, been continuously added to the newer CMIP5 database; pattern-scaling against those newer GCMs can now be undertaken.

Global temperature changes due to atmospheric gas composition that adjusts radiative forcing is achieved through a small number of parameters in a global energy balance model. However aerosols in particular cause problems for this, as the gases are not well-mixed, unlike greenhouse gases. Instead they show strong spatial variation and thus make strong regional
25 variation in radiative forcing, unlike the relatively spatially homogenous greenhouse gases. Shiogama et al. (2010) showed that pattern-scaling is less reliable in the case of precipitation than for temperature in part because precipitation is more sensitive to aerosol forcing. A potential improvement in the presented method in this regard is to use additional spatial masks for aerosol-affected regions.

In terms of many metrics, pattern-scaling is a method that can approximate the vastly more complex GCM frameworks.
30 However this comes with caveats as to its limitations (Good et al., 2015). For example, local climatic feedbacks are not constant in time, and different components of the climate system respond on different timescales (Chadwick & Good, 2013). Nevertheless, as long as used aware of its limitations, its simplicity, availability and computational speed of operation does

allow for intermediate analysis before operation of full-complex GCMs with new land surface parameterisation. This paper takes the further step of adding to its capability the scanning across of a large set of GCMs emulated.

In addition to sources of uncertainty which are linked to methods and the assumptions made, there is uncertainty linked directly to input data quality. For example, the decision to use 20C3M and SRES scenario to derive patterns, and the

5   idealised scenario of 1% annual CO_2 increase to calibrate the EBM model, reflects a compromise between the accuracy of patterns and forcings. It could be argued that ideally both the patterns and the calibration parameters should be derived from the same set of GCM runs. However, since the SRES runs are longer (12 decades with part of the 20C3M run), therefore they are a relatively better source for detection of the linear trend (Mitchel 2003), whereas for one-third of GCMs a necessary alternative would be the idealised scenario of 1% annual CO_2 increase to double levels which provides only 7

10   decades. On the other hand, the idealised CO_2 increase scenarios are a better basis for energy balance model calibration for rigorous studies on the impacts of various CO_2 emission pathways, because the definition of SRES forcings varies between modelling groups (they often encompass atmospheric aerosols) and they are generally poorly documented.

Ultimately, a better dataset is likely to be the CMIP5 ensemble. This formed the basis of the recent 5th IPCC report (IPCC, 2013) using diagnostics available at that time, and is a database only recently completed, has much potential to improve the

15   performance of the described pattern-scaling framework. Aside from the fact that the models themselves have improved, more scenarios are considered, allowing better handling of forcings other than CO_2, and data availability is better. For this reason, the main next enhancement of the IMOGEN system is to migrate over to the CMIP5 dataset. With preparations now starting for the 6th IPCC report, and new simulations being made for that, it is timely to consolidate, and calibrate a new set of patterns for the CMIP5 family of GCMs, building on the analysis presented in this paper.

20   **Data and Code Availability**

The IMOGEN version 2.0 patterns and EBM parameters, along with documentation, are available for full download (under "IMOGEN") from the UK Environmental Information Data Centre (EIDC; http://eidc.ceh.ac.uk). The IMOGEN framework (Huntingford et al. 2010) have become a component of the JULES land surface initiative (Best et al., 2011; Clark et al., 2011), and it is available via that route (jules.jchmr.org). For the most up-to-date IMOGEN code, please contact the

25   corresponding author.

Author Contributions

PZ performed the fitting of the patterns and EBM parameters against the CMIP3 database. CH developed the overall IMOGEN model framework. LMM advised on impacts applications and NS aided with context placing of the analysis in terms of other GCM emulation systems. All authors contributed towards writing the manuscript.

Acknowledgements

We acknowledge the modelling groups, the Program for Climate Model Diagnosis and Intercomparison, and the World Climate Research Programme (WCRP) Working Group on Coupled Modelling for their roles in making available the WCRP Coupled Model Intercomparison Project 3 multi-model dataset. This work was financially supported by the Natural
5   Environment Research Council (UK), pilot project Environmental Virtual Observatory (NE/I002200/1), and by the National Science Centre (Poland), grant SONATA 2014/13/D/ST10/00022. CH was also supported by CEH National Capability funds. We thank Seiji Yukimoto of the Climate Research Department, Meteorological Research Institute, Japan, for assistance in processing MRI-CGCM2.3.2 data.

References

10   Atkin, O. K., Bloomfield, K. J., Reich, P. B., Tjoelker, M. G., Asner, G. P., Bonal, D., Bonisch, G., Bradford, M. G., Cernusak, L. A., Cosio, E. G., Creek, D., Crous, K. Y., Domingues, T. F., Dukes, J. S., Egerton, J. J. G., Evans, J. R., Farquhar, G. D., Fyllas, N. M., Gauthier, P. P. G., Gloor, E., Gimeno, T. E., Griffin, K. L., Guerrieri, R., Heskel, M. A., Huntingford, C., Ishida, F. Y., Kattge, J., Lambers, H., Liddell, M. J., Lloyd, J., Lusk, C. H., Martin, R. E., Maksimov, A. P., Maximov, T. C., Malhi, Y., Medlyn, B. E., Meir, P., Mercado, L. M., Mirotchnick, N., Ng, D., Niinemets, U., O'Sullivan, O.
15   S., Phillips, O. L., Poorter, L., Poot, P., Prentice, I. C., Salinas, N., Rowland, L. M., Ryan, M. G., Sitch, S., Slot, M., Smith, N. G., Turnbull, M. H., VanderWel, M. C., Valladares, F., Veneklaas, E. J., Weerasinghe, L. K., Wirth, C., Wright, I. J., Wythers, K. R., Xiang, J., Xiang, S. and Zaragoza-Castells, J.: Global variability in leaf respiration in relation to climate, plant functional types and leaf traits, New Phytol., 206, 614-636, doi:10.1111/nph.13253, 2015.

Best, M. J. Pryor, M., Clark, D. B., Rooney, G. G., Essery, R. L. H., Menard, C. B., Edwards, J., Hendry, M. A., Porson, A.,
20   Gedney, N., Mercado, L. M., Sitch, S., Blyth, E., Boucher, O., Cox, P. M., Grimmond, C. S. B. and Harding, R. J.: The Joint UK Land Environment Simulator (JULES), model description - Part 1: Energy and water fluxes, Geosci. Model Dev., 4, 677-699, doi:10.5194/gmd-4-677-2011, 2011.

Cabre, M. F., Solman, S. A. and Nunez, M. N.: Creating regional climate change scenarios over southern South America for the 2020's and 2050's using the pattern scaling technique: validity and limitations, Climatic Change, 98, 449-469,
25   doi:10.1007/s10584-009-9737-5, 2010.

Chadwick, R. and Good, P.: Understanding nonlinear tropical precipitation responses to CO_2 forcing, Geophys. Res. Lett., 40, 4911–4915, doi:10.1002/grl.50932, 2013.

Clark, D. B., Mercado, L. M., Sitch, S., Jones, C. D., Gedney, N., Best, M. J., Pryor, M., Rooney, G. G., Essery, R. L. H., Blyth, E., Boucher, O., Harding, R. J., Huntingford, C. and Cox, P. M.: The Joint UK Land Environment Simulator

(JULES), model description - Part 2: Carbon fluxes and vegetation dynamics, Geosci. Model Dev., 4, 701-722, doi:10.5194/gmd-4-701-2011, 2011.

Cox, P. M., Betts, R. A., Collins, M., Harris, P. P., Huntingford, C. and Jones, C. D.: Amazonian forest dieback under climate-carbon cycle projections for the 21st century, Theor. Appl. Climatol., 78, 137-156, doi:10.1007/s00704-004-0049-4, 2004.

Cox, P. M., Betts, R. A., Jones, C. D., Spall, S. A. and Totterdell, I. J.: Acceleration of global warming due to carbon-cycle feedbacks in a coupled climate model, Nature, 408, 184-187, doi:10.1038/35041539, 2000.

Frieler, K., Meinshausen, M., Mengel, M., Braun, N. and Hare, W.: A scaling approach to probabilistic assessment of regional climate change, J. Clim., 25, 3117-3144, doi:10.1175/JCLI-D-11-00199.1, 2012.

Gedney, N., Cox, P. M. and Huntingford, C.: Climate feedback from wetland methane emissions, Geophys. Res. Lett., 31, L20503, doi:10.1029/2004GL020919, 2004.

Good P., Gregory J. M. and Lowe J. A.: A step-response simple climate model to reconstruct and interpret AOGCM projections, Geophys. Res. Lett., 38, L01703, doi:10.1029/2010GL045208, 2011.

Hughes, J. K., Lloyd, A. J., Huntingford, C., Finch, J. W. and Harding, R. J.: The impact of extensive planting of Miscanthus as an energy crop on future CO_2 atmospheric concentrations, Glob. Change Biol. Bioenergy, 2, 79-88, doi:10.1111/j.1757-1707.2010.01042.x, 2010.

Huntingford, C., Booth, B. B. B., Sitch, S., Gedney, N., Lowe, J. A., Liddicoat, S. K., Mercado, L. M., Best, M. J., Weedon, G. P., Fisher, R. A., Lomas, M. R., Good, P., Zelazowski, P., Everitt, A. C., Spessa, A. C., Jones, C. D.: IMOGEN: an intermediate complexity model to evaluate terrestrial impacts of a changing climate, Geosci. Model Dev., 3, 679-687, doi:10.5194/gmd-3-679-2010, 2010.

Huntingford, C. and Cox, P. M.: An analogue model to derive additional climate change scenarios from existing GCM simulations, Clim. Dynam., 16, 575-586, doi:10.1007/s003820000067, 2000.

Huntingford, C., Cox, P. M., Mercado, L. M., Sitch, S., Bellouin, N., Boucher, O. and Gedney, N.: Highly contrasting effects of different climate forcing agents on terrestrial ecosystem services, Philos. T. R. Soc. A, 369, 2026-2037, doi:10.1098/rsta.2010.0314, 2011.

Huntingford, C., Harris, P. P., Gedney, N., Cox, P. M., Betts, R. A., Marengo, J. A. and Gash, J. H. C.: Using a GCM analogue model to investigate the potential for Amazonian forest dieback, Theor. Appl. Climatol., 78, 177-185, doi:10.1007/s00704-004-0051-x, 2004.

Huntingford, C., Mercado, L. and Post, E.: Earth Science The timing of climate change, Nature, 502, 174-175, 2013a.

Huntingford, C., Zelazowski, P., Galbraith, D., Mercado, L. M., Sitch, S., Fisher, R., Lomas, M., Walker, A. P., Jones, C. D., Booth, B. B. B., Malhi, Y., Hemming, D., Kay, G., Good, P., Lewis, S. L., Phillips, O. L., Atkin, O. K., Lloyd, J., Gloor, E., Zaragoza-Castells, J., Meir, P., Betts, R., Harris, P. P., Nobre, C., Marengo, J., Cox, P. M., Simulated resilience of tropical rainforests to CO2-induced climate change, Nat. Geosci., 6, 268-273, doi:10.1038/NGEO1741, 2013b.

Huntingford, C., Smith, D. M., Davies, W. J., Falk, R., Sitch, S. and Mercado, L.M..: Combining the ABA and net photosynthesis-based model equations of stomatal conductance, Ecol. Model., 300, 81-88, doi:10.1016/j.ecolmodel.2015.01.005, 2015.

Ines, A. V. M. and Hansen, J. W.: Bias correction of daily GCM rainfall for crop simulation studies, Agr. Forest Meteorol., 138, 44–53, doi:10.1016/j.agrformet.2006.03.009, 2006.

IPCC: Climate Change 2007: The Physical Science Basis. Contribution of Working Group I to the Fourth Assessment Report of the Intergovernmental Panel on Climate Change [Solomon, S., D. Qin, M. Manning, Z. Chen, M. Marquis, K.B. Averyt, M.Tignor and H.L. Miller (eds.)], Cambridge University Press, Cambridge, United Kingdom and New York, NY, USA., 2007.

IPCC: Climate Change 2013: The Physical Science Basis. Contribution of Working Group I to the Fifth Assessment Report of the Intergovernmental Panel on Climate Change [Stocker, T.F., D. Qin, G.-K. Plattner, M. Tignor, S.K. Allen, J. Boschung, A. Nauels, Y. Xia, V. Bex and P.M. Midgley (eds.)], Cambridge University Press, Cambridge, United Kingdom and New York, NY, USA, 1535 pp, doi:10.1017/CBO9781107415324, 2013.

Joos, F., Bruno, M., Fink, R., Siegenthaler, U., Stocker, T.F. and LeQuere, C.: An efficient and accurate representation of complex oceanic and biospheric models of anthropogenic carbon uptake, Tellus B, 48, 397-417, doi:10.1034/j.1600-0889.1996.t01-2-00006.x, 1996.

Kala, J., De Kauwe, M. G., Pitman, A. J., Lorenz, R., Medlyn, B. E., Wang, Y. P., Lin, Y. S. and Abramowitz, G.: Implementation of an optimal stomatal conductance scheme in the Australian Community Climate Earth Systems Simulator (ACCESS1.3b), Geosci. Model Dev., 8, 3877-3889, doi:10.5194/gmd-8-3877-2015, 2015.

Malhi, Y., Aragao, L. E. O. C., Galbraith, D., Huntingford, C., Fisher, R., Zelazowski, P., Sitch, S., McSweeney, C. and Meir, P.: Exploring the likelihood and mechanism of a climate-change induced dieback of the Amazon rainforest, P. Natl. Acad. Sci. USA, 106, 20610–20615, doi:10.1073/pnas.0804619106, 2009.

Medlyn, B. E., Duursma, R. A., Eamus, D., Ellsworth, D. S., Prentice, I. C., Barton, C. V. M., Crous, K. Y., de Angelis, P., Freeman, M. and Wingate, L.: Reconciling the optimal and empirical approaches to modelling stomatal conductance, Glob. Change Biol., 17, 2134-2144, doi:10.1111/j.1365-2486.2010.02375.x, 2011.

Meehl, G. A., Covey, C., Delworth, T., Latif, M., McAvaney, B., Mitchell, J. F. B., Stouffer, R. J. and Taylor, K. E.: The WCRP CMIP3 multimodel dataset – A new era in climate change research, B. Am. Meteorol. Soc., 88, 1383–1394, doi:10.1175/BAMS-88-9-1383, 2007.

Meehl, G. A., T. F. Stocker, W. D. Collins, P. Friedlingstein, A. T. Gaye, J. M. Gregory, A. Kitoh, R. Knutti, J. M. Murphy, A. Noda, S. C. B. Raper, I. G. Watterson, A. J. Weaver and Z.-C. Zhao: Global Climate Projections. In: Climate Change 2007: The Physical Science Basis. Contribution of Working Group I to the Fourth Assessment Report of the Intergovernmental Panel on Climate Change [Solomon, S., D. Qin, M. Manning, Z. Chen, M. Marquis, K. B. Averyt, M. Tignor and H. L. Miller (eds.)], Cambridge University Press, Cambridge, United Kingdom and New York, NY, USA., 2007.

Mercado, L. M., Bellouin, N., Sitch, S., Boucher, O., Huntingford, C., Wild, M. and Cox, P. M.: Impact of changes in diffuse radiation on the global land carbon sink, Nature, 458, 1014-U87, doi:10.1038/nature07949, 2009.

Mercado, L. M., Huntingford, C., Gash, J. H. C., Cox, P. M. and Jogireddy, V.: Improving the representation of radiation interception and photosynthesis for climate model applications, Tellus B, 59, 553-565, doi:10.1111/j.1600-0889.2007.00256.x, 2007.

Mercado, L. M., Patino, S., Domingues, T. F., Fyllas, N. M., Weedon, G. P., Sitch, S., Quesada, C. A., Phillips, O. L., Aragao, L. E. O. C., Malhi, Y., Dolman, A. J., Restrepo-Coupe, N., Saleska, S. R., Baker, T. R., Almeida, S., Higuchi, N. and Lloyd, J.: Variations in Amazon forest productivity correlated with foliar nutrients and modelled rates of photosynthetic carbon supply, Philos. T. R. Soc. B, 366, 3316-3329, doi:10.1098/rstb.2011.0045, 2011.

Mercado L. M, et al., Sensitivity of future land carbon storage to thermal acclimation of photosynthesis in climate-carbon cycle models. In Preparation.

Mitchell, J. F. B., Johns, T. C., Eagles, M., Ingram, W. J. and Davis, R. A.: Towards the construction of climate change scenarios, Climatic Change, 41, 547-581, doi:10.1023/A:1005466909820, 1999.

Mitchell, T. D.: Pattern scaling - An examination of the accuracy of the technique for describing future climates, Climatic Change, 60, 217-242, doi:10.1023/A:1026035305597, 2003.

Mitchell, T. D. and Jones, P. D.: An improved method of constructing a database of monthly climate observations and associated high-resolution grids, Int. J. Climatol., 25, 693-712, doi:10.1002/joc.1181, 2005.

Moorcroft, P. R., Hurtt, G. C. and Pacala, S. W.: A method for scaling vegetation dynamics: The ecosystem demography model (ED), Ecol. Monogr., 71, 557-585, doi:10.1890/0012-9615(2001)071[0557:AMFSVD]2.0.CO;2, 2001.

Nakićenović, N., Alcamo, J., Davis, G. et al: IPCC Special Report on Emissions Scenarios, Cambridge University Press, Cambridge, UK, 570 pp., 2000.

5   Shiogama, H., Emori, S., Takahashi, K., Nagashima, T., Ogura, T., Nozawa, T. and Takemura, T.: Emission scenario dependency of precipitation on global warming in the MIROC3.2 model, J. Climate, 23, 2404-2417, doi:10.1175/2009JCLI3428.1, 2010.

Sitch, S., Cox, P. M., Collins, W. J. and Huntingford, C.: Indirect radiative forcing of climate change through ozone effects on the land-carbon sink, Nature, 448, 791-U4, doi:10.1038/nature06059, 2007.

10 Sitch, S., Huntingford, C., Gedney, N., Levy, P. E., Lomas, M., Piao, S. L., Betts, R., Ciais, P., Cox, P., Friedlingstein, P., Jones, C. D., Prentice, I. C. and Woodward, F. I.: Evaluation of the terrestrial carbon cycle, future plant geography and climate-carbon cycle feedbacks using five Dynamic Global Vegetation Models (DGVMs), Glob. Change Biol., 14, 2015-2039, doi: 10.1111/j.1365-2486.2008.01626.x, 2008.

Smith, B., Prentice, I. C., and Sykes, M. T.: Representation of Vegetation Dynamics in the Modelling of Terrestrial
15 Ecosystems: Comparing Two Contrasting Approaches within European Climate Space, Global Ecol. and Biogeogr., 10, 621-637, doi:10.1046/j.1466-822X.2001.t01-1-00256.x, 2001.

Smith, N. G. and Dukes, J. S.: Plant respiration and photosynthesis in global-scale models: incorporating acclimation to temperature and CO2, Glob. Change Biol., 19, 45–63, doi:10.1111/j.1365-2486.2012.02797.x, 2013.

Sperry, J. S., Wang, Y., Wolfe, B. T., Mackay, D. S., Anderegg, W. R. L., McDowell, N. G. and Pockman, W. T.: Pragmatic
20 hydraulic theory predicts stomatal responses to climatic water deficits, New Phytol., doi: 10.1111/nph.14059, 2016.

Taylor, K. E., Stouffer, R. J. and Meehl, G. A.: An overview of CMIP5 and the experiment design, B. Am. Meteorol. Soc., 93, 485-498, doi:10.1175/BAMS-D-11-00094.1, 2012.

Verheijen L. M., Aerts, R., Brovkin, V., Cavender-Bares, J., Cornelissen, J. H. C., Kattge, J. and Van Bodegom, PM: Inclusion of ecologically based variation in plant functional types reduces the projected land carbon sink in an earth system
25 model, Glob. Change Biol., 21, 3074-3086, doi: 10.1111/gcb.12871, 2015.

Wigley, T. M. L., Raper, S. C. B., Smith, S. and Hulme, M.: The Magicc/ScenGen Climate Scenario Generator: version 2.4, Technical manual. CRU, UEA, Norwich, U.K., 2000.

Zaehle, S., Friedlingstein, P. and Friend, A. D.: Terrestrial nitrogen feedbacks may accelerate future climate change, Geophys. Res. Lett., 37, L01401, doi:10.1029/2009GL041345, 2010.

Zelazowski, P., Malhi, Y., Huntingford, C., Sitch, S. and Fisher, J. B.: Changes in the potential distribution of humid tropical forests on a warmer planet, Philos. T. R. Soc. A, 369, 137-160, doi:10.1098/rsta.2010.0238, 2011.

Table 1. **Availability of WCRP CMIP3 data for the climate patterns study, and characteristics of models' depiction of land and water areas (variable sftlf).** Land/water transition is either continuous (*cont.*) or abrupt (binary mask - *bin.*). The first characteristic in column "Land mask" pertains to coastlines, whereas the second – to inland waters. The codes in column "Data gaps and issues" are: M – missing, E – 4D variable (surface values need to be extrapolated), G – data gaps, R – some data needed resizing.

	GCM name	Origin	Land mask	Resolution	Data gaps and issues
1.	BCCR-BCM2.0	Norway	cont./cont.	64x128	E (HUR)
2.	CGCM3.1(T47)	Canada	bin./bin.	48x96	E (HUR)
3.	CNRM-CM3	France	bin./bin.	64x128	E (HUR)
4.	CSIRO-Mk3.0	Australia	bin./bin.	96x192	M (UAS, VAS, PS)
5.	CSIRO-Mk3.5	Australia	bin./bin.	96x192	E (HUR)
6.	GFDL-CM2.0	USA	cont./bin.	90x144	E (HUR)
7.	GFDL-CM2.1	USA	cont./bin.	90x144	E (HUR)
8.	GISS-EH	USA	bin./cont.	46x72	E (HUR)
9.	GISS-ER	USA	bin./cont.	46x72	E (HUR), M (RLDS)
10.	FGOALS-g1.0	China	cont./bin.	60x128	E (HUR)
11.	INGV-SXG	Italy	bin./bin.	160x320	E (HUR, UAS, VAS), M (RLDS, RSDS)
12.	INM-CM3.0	Russia	bin./bin.	45x72	E (HUR)
13.	IPSL-CM4	France	cont./bin.	72x96	E (HUR)
14.	MIROC3.2(hires)	Japan	cont./cont.	160x320	E (HUR)
15.	MIROC3.2(medres)	Japan	cont./bin.	64x128	E (HUR)
16.	ECHO-G	Germany-Korea	bin/bin.	48x96	M (HUR)
17.	ECHAM5/MPI-OM	Germany	cont./bin.	96x192	E (HUR)
18.	MRI-CGCM2.3.2	Japan	cont./cont.	64x128	E (HUR) G (PRSN)
19.	CCSM3	USA	cont./bin.	128x256	E (HUR, UAS, VAS)
20.	PCM	USA	cont./bin.	64x128	E (HUR, UAS, VAS)
21.	UKMO-HadCM3	UK	bin/bin.	73x96	E (HUR)
22.	UKMO-HadGEM1	UK	cont./bin.	145x192	E (HUR), R (UAS,VAS)

Table 2. Calibration parameters of the simple IMOGEN Energy Balance Model, for each considered Global Circulation Model.
The first column presents which runs (experiments) were used to derive the parameters, listed in the following columns: (i) an ocean effective thermal diffusivity which determines the uptake of energy, κ (Wm^{-1}K^{-1}), (ii) a constant ratio of mean land and ocean surface (SST) rate of warming, ν, (iii-iv) climate sensitivity over land λ_l and ocean λ_o (W m^{-2} K^{-1}), and (v) f, which is a land fraction, including Antarctica, f. The last column presents GCM-specific ratios of warming aver all land per degree of global warming.

	GCM	Calibration basis	Pattern basis	λl	λo	κ	ν	f	ΔTl/°K
1.	BCCR-BCM2.0	pictrl, 1% to2x	SRES A2	2.00	2.30	350	1.40	0.28	1.26
2.	CGCM3.1(T47)	pictrl, 1% to4x	SRES A2	1.50	1.30	270	1.50	0.31	1.30
3.	CNRM-CM3	pictrl, 1% to4x	SRES A2	1.65	1.58	500	1.46	0.28	1.29
4.	CSIRO-Mk3.0	pictrl, 1% to2x	SRES A2	1.20	1.25	2800	1.69	0.29	1.41
5.	CSIRO-Mk3.5	pictrl, 1% to2x	SRES A2	1.35	0.80	1300	1.58	0.29	1.35
6.	GFDL-CM2.0	pictrl, 1% to4x	SRES A2	1.15	1.70	510	1.53	0.30	1.32
7.	GFDL-CM2.1	pictrl, 1% to4x	SRES A2	1.15	2.05	460	1.58	0.30	1.35
8.	GISS-EH	pictrl, 1% to2x	SRES A1B	1.30	1.65	520	1.48	0.29	1.30
9.	GISS-ER	pictrl, 1% to4x	SRES A2	1.05	1.40	1200	1.61	0.29	1.37
10.	FGOALS-g1.0	pictrl, 1% to2x	SRES A1B	1.80	2.80	11000	1.47	0.30	1.46
11.	INGV-SXG	pictrl, 1% to4x	SRES A2	0.70	1.90	320	1.65	0.28	1.39
12.	INM-CM3.0	pictrl, 1% to4x	SRES A2	1.35	1.70	500	1.50	0.30	1.30
13.	IPSL-CM4	pictrl, 1% to4x	SRES A2	1.00	1.10	700	1.57	0.30	1.34
14.	MIROC3.2(hires)	pictrl, 1% to2x	SRES A1B	1.00	0.70	510	1.38	0.29	1.24
15.	MIROC3.2(medres)	pictrl, 1% to4x	SRES A2	0.83	1.00	720	1.57	0.29	1.35
16.	ECHO-G	pdctrl, 1% to4x	SRES A2	1.05	1.80	50	1.76	0.29	1.45
17.	ECHAM5/MPI-OM	pictrl, 1% to4x	SRES A2	0.86	0.95	500	1.60	0.29	1.36
18.	MRI-CGCM2.3.2	pdctrl, 1% to4x	SRES A2	1.68	1.25	380	1.38	0.30	1.22
19.	CCSM3	pdctrl, 1% to4x	SRES A2	1.10	1.70	1200	1.47	0.29	1.29
20.	PCM	pdctrl, 1% to4x	SRES A2	1.95	2.30	720	1.43	0.29	1.27
21.	UKMO-HadCM3	pictrl, 1% to2x	SRES A2	0.40	1.85	270	1.78	0.29	1.45
22.	UKMO-HadGEM1	pictrl, 1% to4x	SRES A2	0.92	1.46	480	1.60	0.29	1.36
	All			1.23±0.40	1.57±0.51	1148±2220	1.55±0.11	0.29±0.01	1.34±0.06

Table 3. Mean climate change patterns (change in quantity per degree of global warming). Values in italics are across-ensemble averages used to fill in data gaps. In these cases, the Percentage Variance Explained statistic was not calculated. Across-variables summary values (last column) which concern incomplete sets of variables are in square brackets.

	GCM name	TAS	HUR	UAS+VAS	RLDS	RSDS	PR	PRSN	PS	ALL
1.	BCCR-BCM2.0	1.0463 (83.04)	-0.0201 (13.29)	0.0089 (2.66)	5.6754 (76.51)	-0.6185 (9.73)	0.0300 (8.16)	-0.0025 (13.14)	0.2324 (30.70)	29.65
2.	CGCM3.1(T47)	1.0561 (85.79)	0.0974 (19.80)	0.0197 (8.30)	6.0605 (87.28)	-0.4722 (18.82)	0.0448 (18.71)	-0.0015 (16.66)	0.0730 (21.33)	34.59
3.	CNRM-CM3	1.0371 (86.64)	-0.0111 (24.84)	0.0098 (8.73)	5.7499 (81.41)	-0.4978 (19.65)	0.0255 (17.05)	0.0000 (17.35)	0.1838 (38.48)	36.77
4.	CSIRO-Mk3.0	1.0740 (82.73)	-0.2354 (13.99)	*0.0108* *(-)*	5.9023 (84.39)	-0.6072 (24.46)	0.0165 (9.38)	-0.0032 (25.70)	*0.0947* *(-)*	[40.11]
5.	CSIRO-Mk3.5	1.0270 (87.73)	-0.2214 (17.04)	0.0059 (6.93)	6.2917 (87.92)	-0.3596 (25.23)	0.0044 (12.42)	-0.0035 (17.22)	0.0138 (21.94)	34.56
6.	GFDL-CM2.0	1.0731 (83.58)	-0.2653 (14.77)	0.0071 (8.25)	6.0471 (83.69)	-1.8451 (34.58)	0.0042 (16.89)	-0.0041 (21.49)	0.0657 (24.35)	35.95
7.	GFDL-CM2.1	1.0794 (79.71)	-0.2310 (17.35)	0.0113 (9.59)	6.2023 (82.62)	-1.7225 (33.21)	-0.0017 (17.93)	-0.0067 (18.66)	0.2057 (29.21)	36.03
8.	GISS-EH	1.0543 (75.71)	0.0080 (10.48)	0.0103 (4.25)	6.6734 (77.09)	-1.4802 (1.95)	0.0415 (11.28)	-0.0016 (8.04)	0.0264 (12.18)	25.12
9.	GISS-ER	1.0365 (80.07)	-0.1572 (17.25)	0.0099 (7.08)	*6.1883* *(-)*	-0.9399 (11.05)	0.0384 (14.76)	-0.0018 (10.16)	0.0251 (18.31)	[22.67]
10.	FGOALS-g1.0	1.1180 (83.05)	-0.0980 (4.11)	-0.0031 (1.36)	6.3137 (82.71)	-0.9748 (9.67)	0.0205 (6.70)	-0.0010 (15.52)	0.0836 (13.62)	27.09
11.	INGV-SXG	1.0863 (88.01)	-0.0209 (22.96)	0.0128 (5.20)	*6.2418* *(-)*	*-0.7667* *(-)*	0.0184 (10.68)	-0.0067 (19.10)	0.0217 (18.58)	35.98
12.	INM-CM3.0	1.0604 (83.51)	-0.0391 (15.44)	0.0130 (4.88)	5.7124 (78.17)	-0.2908 (23.54)	0.0200 (14.32)	-0.0071 (12.97)	0.0124 (16.43)	31.16
13.	IPSL-CM4	1.1043 (90.18)	-0.6717 (27.46)	0.0059 (9.92)	6.1517 (85.26)	0.0932 (27.85)	0.0166 (15.72)	-0.0089 (23.73)	0.1216 (21.31)	37.68
14.	MIROC3.2(hires)	1.0801 (94.19)	-0.1528 (16.89)	0.0031 (8.45)	6.2088 (92.28)	-1.0731 (36.21)	0.0271 (20.90)	-0.0052 (25.45)	0.2352 (37.87)	41.53
15.	MIROC3.2(medres)	1.1281 (91.16)	-0.2819 (15.56)	0.0062 (9.38)	6.4687 (88.97)	-1.7130 (38.30)	0.0272 (22.37)	-0.0032 (23.53)	0.1417 (30.26)	39.94
16.	ECHO-G	1.1383 (88.41)	*-0.1256* *(-)*	0.0165 (9.54)	6.5682 (86.84)	-1.4149 (20.41)	0.0574 (18.77)	-0.0046 (21.54)	-0.0648 (19.65)	[37.88]
17.	ECHAM5/MPI-OM	1.0726 (89.81)	-0.2200 (18.66)	0.0173 (8.35)	6.1048 (89.35)	-0.3009 (18.78)	0.0294 (14.08)	-0.0052 (17.45)	0.0714 (22.61)	34.89
18.	MRI-CGCM2.3.2	1.0641 (84.62)	0.6378 (13.21)	-0.0048 (3.25)	6.5956 (82.92)	-1.2903 (10.43)	0.0387 (7.60)	*-0.0063* *(-)*	0.0979 (17.37)	[31.34]
19.	CCSM3	1.1182 (87.92)	-0.0307 (15.09)	0.0091 (6.75)	6.8102 (89.67)	-1.2080 (24.48)	0.0477 (21.47)	-0.0071 (20.45)	0.1629 (25.02)	36.36
20.	PCM	1.1059 (78.64)	0.0704 (9.65)	0.0346 (1.13)	6.2678 (75.20)	-0.9678 (8.34)	0.0573 (12.52)	0.0009 (13.56)	0.1509 (17.32)	27.04
21.	UKMO-HadCM3	1.0572 (86.57)	-0.7051 (29.40)	0.0137 (9.85)	5.6891 (84.81)	0.2089 (27.15)	0.0096 (16.36)	-0.0036 (15.88)	-0.0542 (23.05)	36.63
22.	UKMO-HadGEM1	1.1222 (88.60)	-0.0900 (18.05)	0.0190 (15.49)	6.2180 (89.33)	-1.9194 (37.04)	0.0076 (21.45)	-0.0039 (22.27)	0.1814 (32.21)	40.55
	ALL	1.079 ±0.032 (85.44 ±4.37)	-0.1256 ±0.2579 (16.92 ±5.71)	0.0108 ±0.0080 (7.11 ±3.32)	6.188 ±0.400 (84.74 ±4.97)	-0.9164 ±0.6000 (23.29 ±10.23)	0.0264 ±0.0165 (14.98 ±4.61)	-0.0040 ±0.0025 (17.96 ±4.67)	0.095 ±0.084 (23.33 ±6.99)	(34.25 ±5.21)
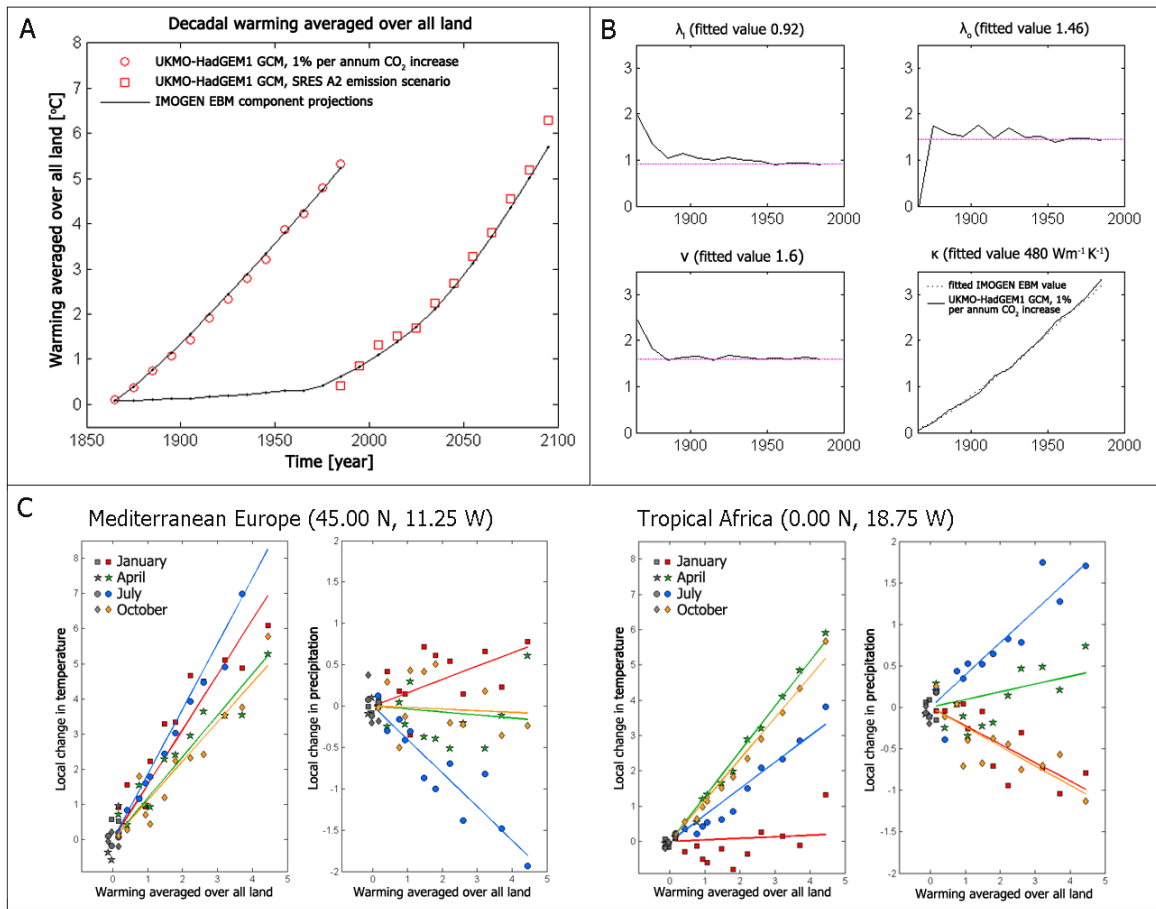
Figure 1: Illustration of the process leading to parameterization of the IMOGEN Energy Balance Model and the scaled climate patterns (together forming the "pattern scaling set"), based on the example of the UKMO-HadGEM1 GCM. A: emulation of a warming pathway across time. The 1% to quadrupling atmospheric CO_2 run was used for calibration of the energy balance model while the SRES A2 scenario run was used to validate the results. **B**: Fitting of the individual EBM parameters, underlining the match presented in A. Climate sensitivities over land λ_l and ocean λ_o, as well as the ratio of land to ocean warming rate, ν, (pink lines) are derived directly from GCM run data (black curves, 1% run). The fourth parameter, an ocean effective thermal diffusivity, κ, determines modelled oceanic temperature profile. The κ value is selected based upon comparing calculated values of top-of-profile temperature against global mean SST changes projected by UKMO-HadGEM1 1% run (shown). **C**: Example local fitting of patterns of temperature and precipitation, found as regression coefficients (coloured straight lines) against calculated changes in mean temperature over land from UKMO-HadGEM1. Two representative grid-boxes in Mediterranean Europe and Tropical Africa are shown. Coloured symbols are decadal mean monthly values from the UKMO-HadGEM1 SRES A2 run, whilst the grey markers represent data from the 20C3M simulation, which were used to normalize to temperature and precipitation change, and are also corresponding to CRU normals (years 1961–90). Regression "pattern" fit is forced through [0,0] point, as in diagrams.
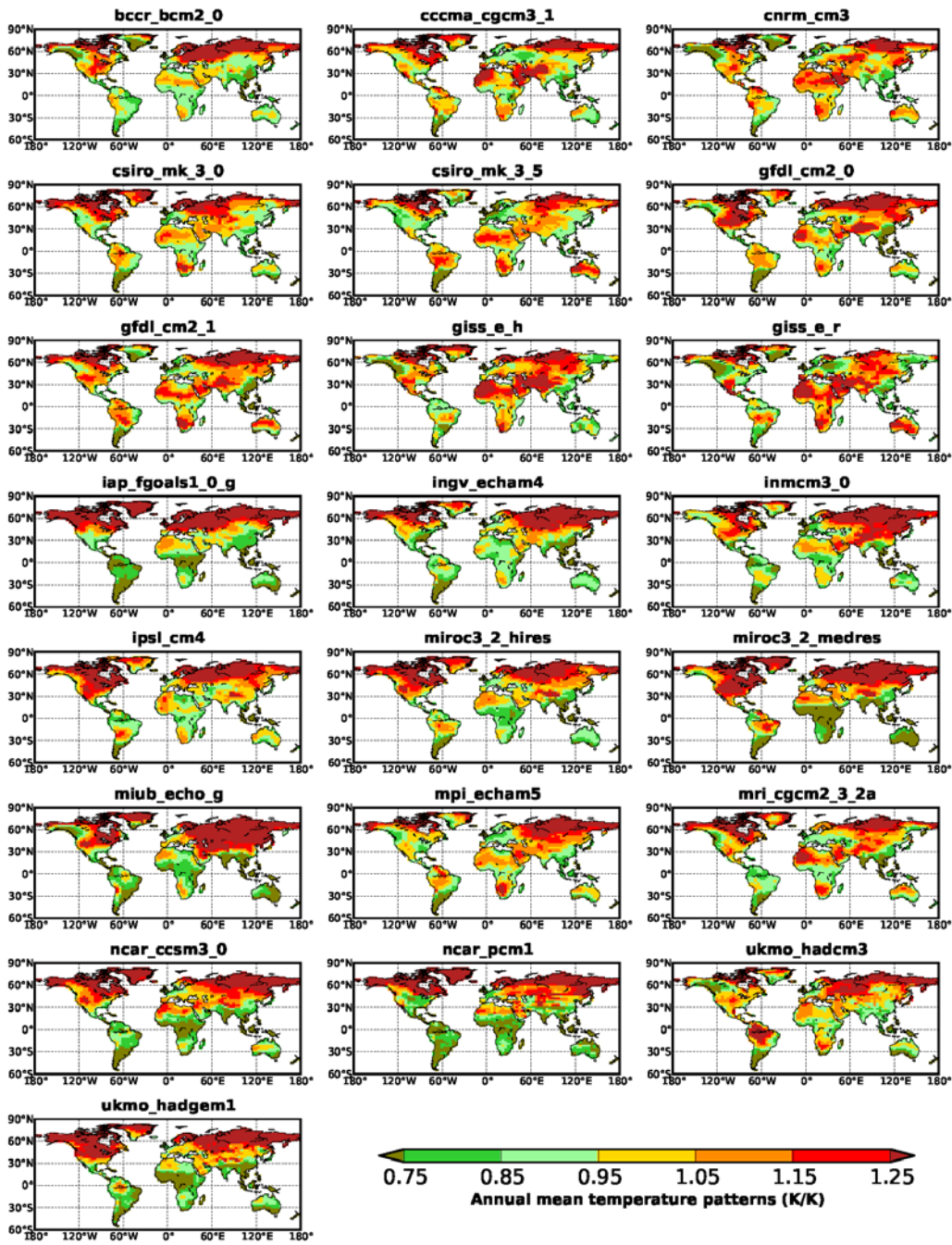
Figure 2: Annual means of the monthly patterns of local temperature change per degree warming over all land (K K⁻¹). Data presented for 22 GCMs considered in this study.
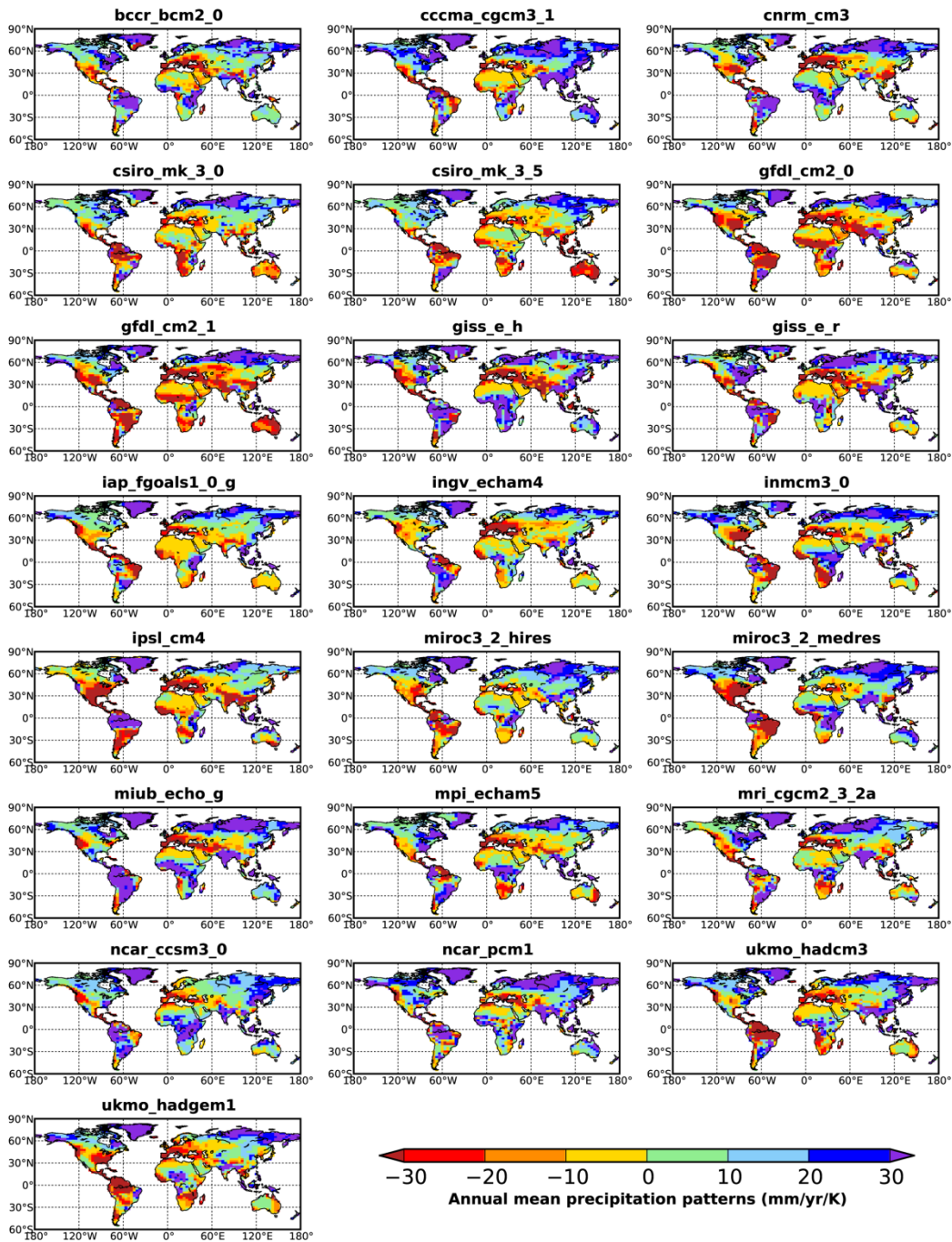
Figure 3: Annual means of the monthly patterns of local precipitation change per degree warming over all land (mm yr^{-1} K^{-1}). Data presented for 22 GCMs considered in this study**.**
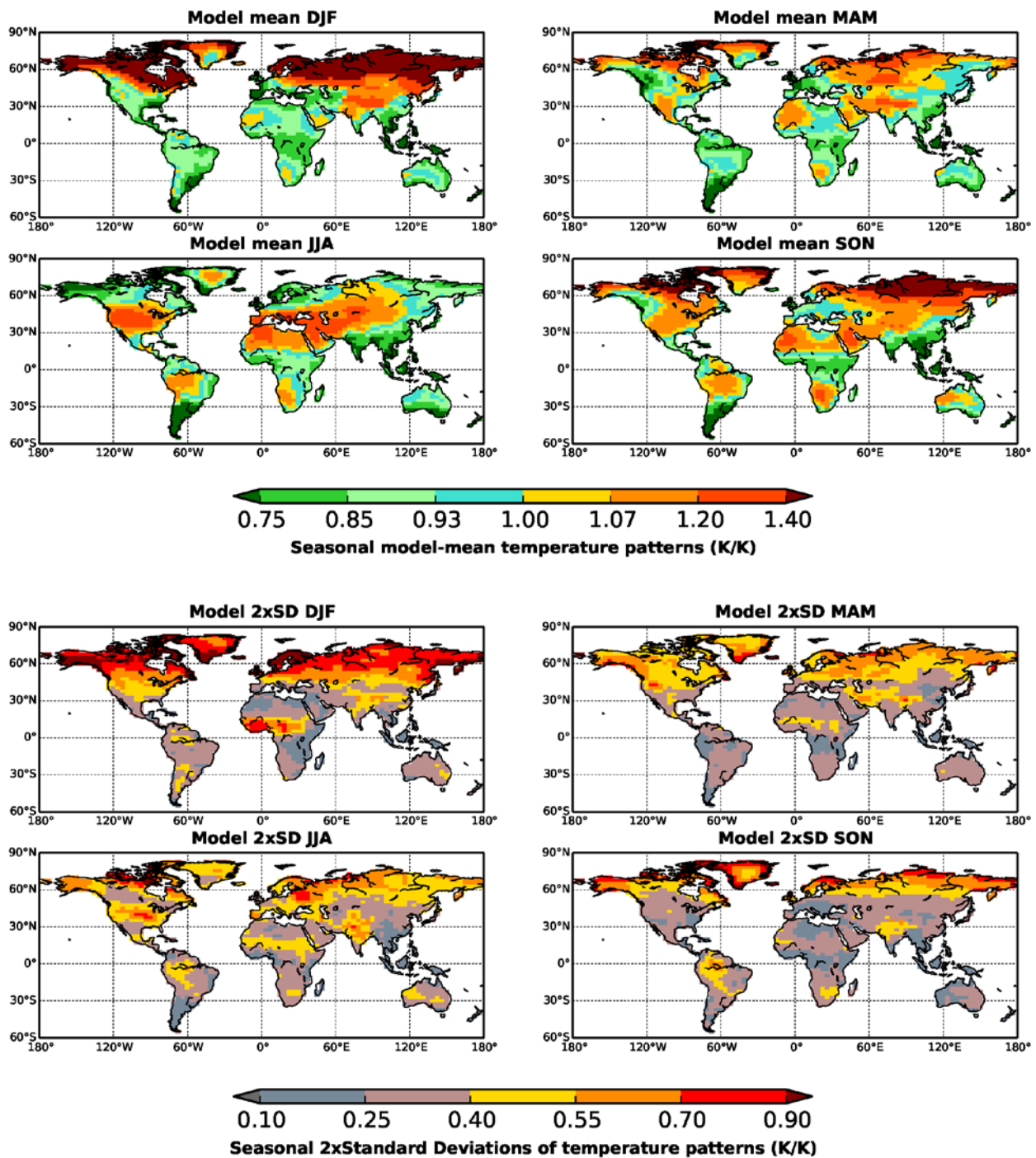
Figure 4: Seasonal means and variation (2*SD) of the monthly patterns of local temperature change per degree warming over all land (K K^{-1}), across 22 GCMs.
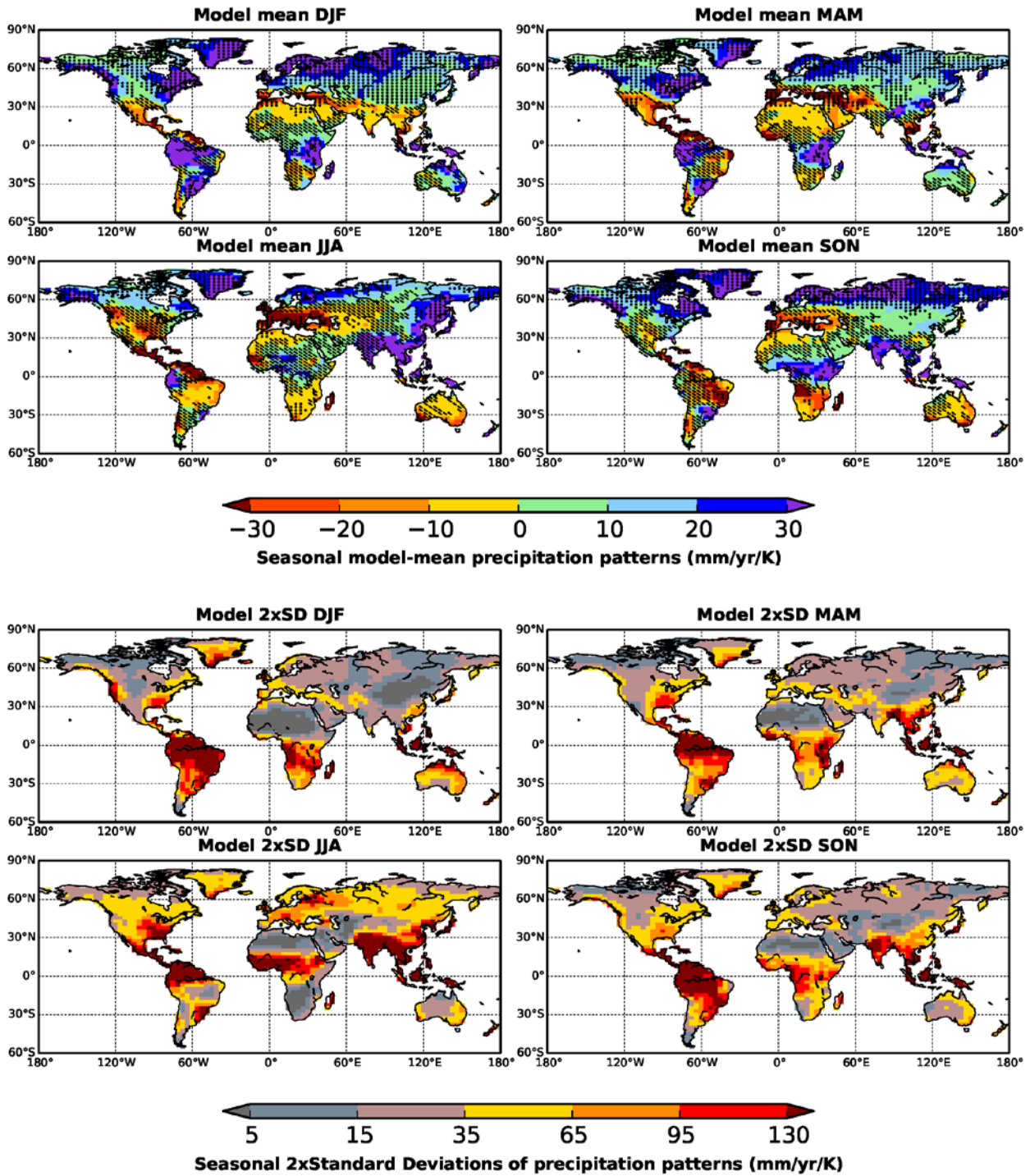
Figure 5: Seasonal means and variation (2*SD) in the monthly patterns of local precipitation change per degree warming over all land (mm yr-1 K-1), across 22 GCMs. In regions marked with stippling more than 66% of the models agree in the sign of the change.
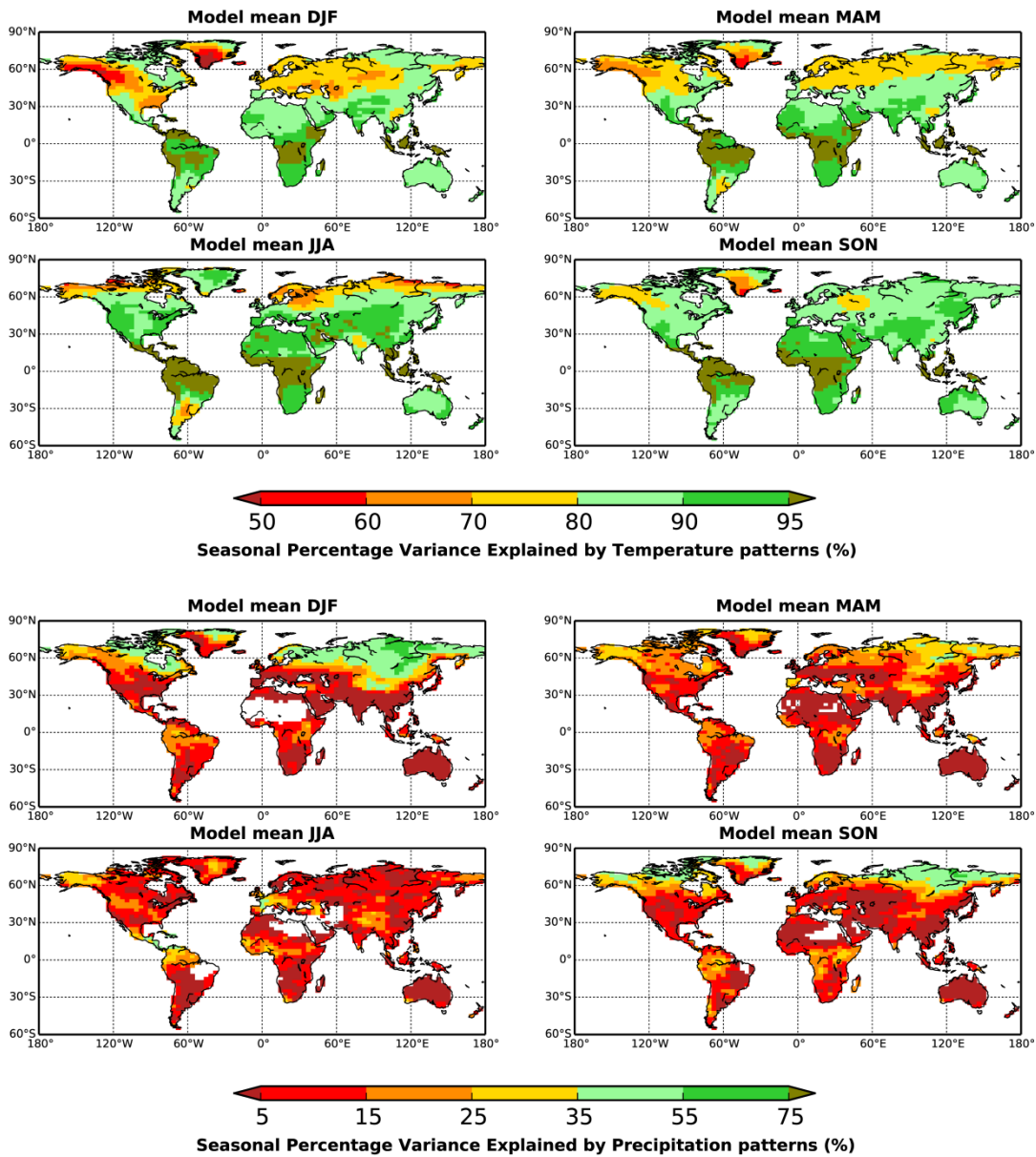
Figure 6: Seasonal coefficient of determination (COD) of the monthly patterns of local temperature and precipitation change per degree warming, across 22 GCMs.
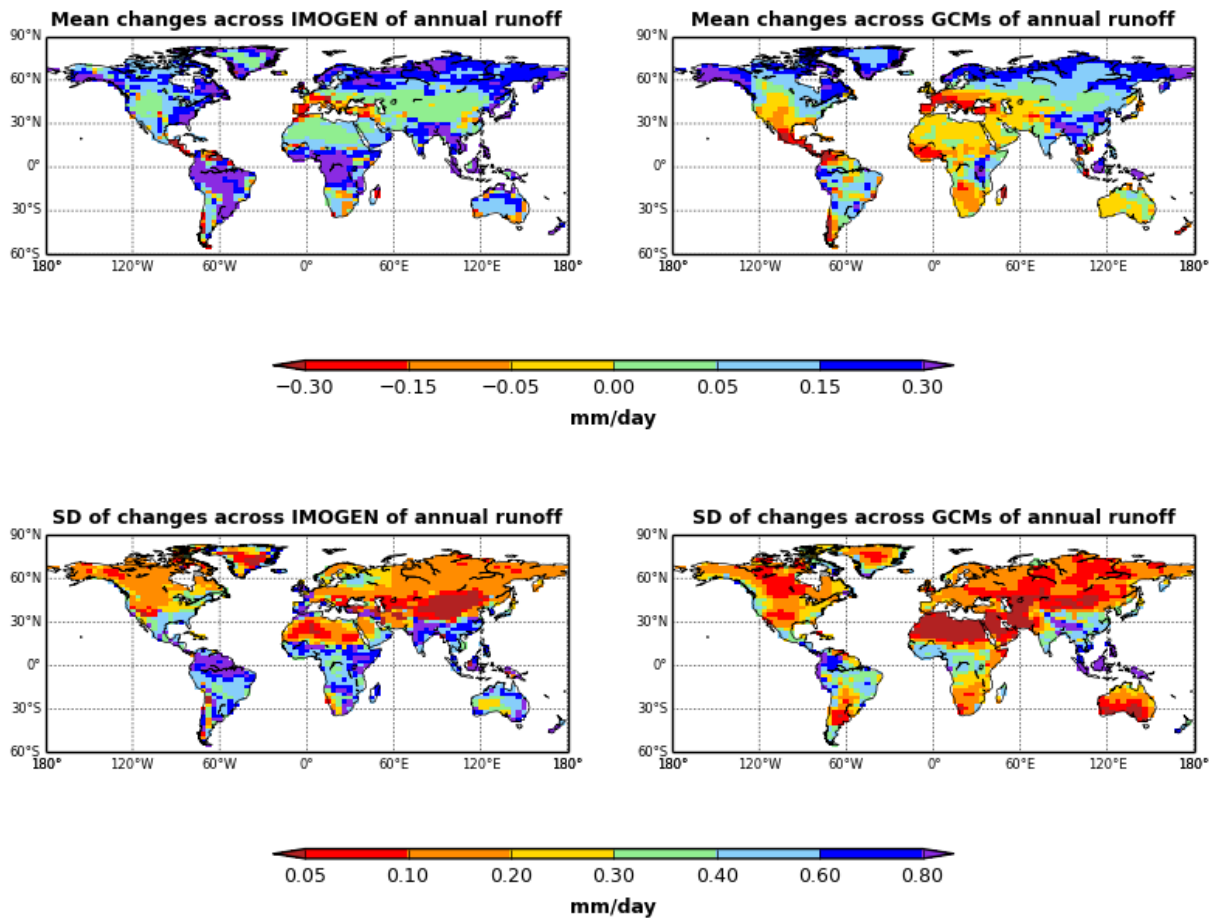
Figure 7. Comparison of IMOGEN and GCM estimates of annual mean runoff changes (20 years centred 2090 minus 20 years centred 1900), and for emissions scenario SRESA1B. Top left panel is the mean changes in runoff across GCMs emulated in the IMOGEN system, all forcing the JULES land surface model. Top right panel is the mean changes in runoff as taken directly from the GCMs themselves. In the bottom left panel, at each gridbox, presented is the SD of changes in runoff for IMOGEN, again across GCMs emulated. Bottom right panel is SD of changes in runoff taken directly from the GCMs.